Journal of the Iranian Chemical Society (2019) 16:695–705
https://doi.org/10.1007/s13738-018-1546-1

ORIGINAL PAPER

A new effective nano-adsorbent and antibacterial material of hydroxyapatite

Mohammad Chahkandi[1] · Seyedeh Roghayyeh Saadatdar Arami[1] · Masoud Mirzaei[2] · Behnam Mahdavi[1] · Seyed Mahmod Hosseini-Tabar[1]

Received: 30 May 2018 / Accepted: 7 November 2018 / Published online: 16 November 2018

Abstract
In the present work, nano-particles of potassium-substituted hydroxyapatite with formula of $(Ca_{2.94}K_{2.06})(PO_4)_{0.94}(CO_3)_{2.06}(OH)$ (KHA) are reported showing effective adsorption of Congo red dye in the room temperature. Synthesized sol–gel-derived KHA was identified by XRD, FTIR, TGA/DTA, and EDXA analyses. Moreover, the size of nano-particles and micro-strain of the synthesized KHA were measured using Williamson–Hall (W–H) plots and TEM in amount of 65–70 nm. The capacity of equilibrium adsorption (q_m) for 100 ppm of Congo red was evaluated as high as 505.19 mg g^{-1} under optimum conditions. The adsorption charts and kinetic results obtained at ambient conditions well fitted with the Langmuir equation and the pseudo–first–order model with correlation coefficients of 0.9939 and 0.9867, respectively. The obtained results obviously show that the new synthesized KHA can be used for industrial wastewater purification in a good manner. The title nano-material also shows excellent antibacterial activity as highly prevention of bacteria strain growth with the lowest concentration of 125 µg/mL.

Keywords Potassium-substituted nano-particle of hydroxyapatite · Sol–gel · Congo red · Kinetics · Adsorption isotherms · Antibacterial activity

Introduction

The synthetic organic compounds are commonly present in the wastewaters of industries that make serious obstacles such as human health, make slowing of micro-organisms growing, and carcinogenic and mutagenic for aquatic systems [1, 2]. They often contain aromatic rings make them stable and toxic (causing health and visibility problems) and cannot be completely removed from environmental wastewaters [3]. Therefore, several methods of dye removing from aqueous solution are used including chemical reduction and oxidation, precipitation, electrochemical, and adsorption ones [4–8]. However, applying inorganic or/and organic adsorbents, because of simplicity, low energy, without generating toxic sludge, can be applied as an effective method [9]. A diazo dye called Congo red (CR) (CR) (sodium salt of benzidinediazobis-1-naphthylamine-4-sulfonic acid) with good water solubility is an anionic color commonly used in textile industries and as the *p*H indicator. However, solubility of CR in water resulted in some difficulty for discoloring, while adsorption method can handle this challenge [10–13]. In the last years, azo dyes elimination like CR by different adsorbent materials as bentonite, $CuFe_2O_4$, nano-porous silica, fly ash, kaolin, marble powder, and some more have been researched [14–16]. Most of the above-mentioned compounds do not show highly capacity of adsorption (under 100 mg/g) within CR molecules. Therefore, other alternative adsorbents are used, such as calcium phosphate (Ca-P) including calcium hydroxyapatite (CaHA) owing to low-cost, and highly effective for removing the pollutants [10–13, 17–19]. CaHA and its derivatives possess two ionic binding sites as C, full of calcium ions (positive charge) and P, and full of phosphate ions (negative charge) within the unit cell surfaces [20]. Therefore, the anionic CR dye can be electrostatically attracted on C sites [10–13]. Therefore, the title material has been used as contaminates removal from wastewater such as

✉ Mohammad Chahkandi
m.chahkandi@hsu.ac.ir

✉ Masoud Mirzaei
mirzaeesh@um.ac.ir

[1] Department of Chemistry, Hakim Sabzevari University, 96179-76487 Sabzevar, Iran

[2] Department of Chemistry, Faculty of Science, Ferdowsi University of Mashhad, 917751436 Mashhad, Iran

cationic and anionic proteins, azo dyes, and phenols [21–23]. It should be mentioned that there are not any reports concerning CR adsorption by sol–gel-prepared KHA in the literature.

As an extension of our continued interest in the preparation of new nano-materials bearing some potential applications like separation, environmental photocatalytic degradation of dye and organic pollutants [23–30], herein, a new KHA was for the first time synthesized by the sol–gel method showing as the efficient adsorbent for CR. During the past decade, since cation-doped HAPs, that is, substitution of calcium ions, phosphate groups, and hydroxyl groups in the structure of HAp is possible, so it has opened up a new area of various applications like bio-medical, dentistry, and purification systems [30]. For instance, copper substituted HAp for the uranium [31], Ag-doped HAp for the CR [32], HAp loaded with strontium for the soybean oil [33], and silicon doped HAp for copper [34] adsorption, and so on can be mentioned. Potassium has capability in the regulation of bio-chemical and apatite mineral nucleation processes [35, 36] and K-substituted HAp could also show better function than the individual HAp or β-tricalcium phosphate [37].

In this work, sol–gel method is applied to prepare the nano-structure of K-substituted HAp (KHA) that bearing the simplicity, high purity of product, sufficiency to make nano-particles, and low crystallinity of product with efficient capacity of absorption. As mentioned, doping of potassium has been resulted in scientific bioactivity points of synthesized KHA (lowest concentration of 125 µg/mL makes highly prevention of bacteria strains growth; see "Antibacterial study" section). Moreover, this synthesized KHA shows the permanent capacities of CR dye adsorption at RT (maximum adsorption capacity (q_m) = 505.2 mg/g; see "Assessment of performance" section) in comparison with the other reported adsorbents without needing for changing of *p*H or temperature. The material was characterized by powder X-ray diffraction (XRD), Fourier transform infrared (FTIR) analysis, and also its particle size to be estimated by XRD and TEM. Moreover, thermogravimetric/differential thermal analysis (TGA/DTA) about synthesized KHA has been done. Finally, the adsorption capability of the KHA studied within aqueous solutions of CR dye at different temperature and adjusting pH values of treatment solutions. The kinetics and equilibrium isotherms of CR adsorption together with antibacterial activity as highly prevention of bacteria strains growth will be discussed in detail.

Experimental section

KHA sol–gel preparation and measurement of physical analysis

First of all, 24 h hydrolysis process about triethyl phosphate ($(C_2H_5O)_3PO$, TEP, Fluka) at R. T. was performed. Then, the 3M aqueous solution of $Ca(NO_3)_2{\cdot}4H_2O$ (Merck) and 3M KNO_3 (28 w/w% K) was added to 4M TEP (molar ration of Ca + K to $P = 1.67$) with the rate of 6 mL/min. Next, the respected solution for 60 min was strongly mixed up at 80 °C. Eventually, 48 h aging process at R. T. about obtained clear solution was done. After that, the drying process at 100 °C was done that resulted in a white dried powder and in following low temperature of calcination process at 300 °C with 2°C/min constant heat rate was executed. The prepared powder of KHA was characterized by the X-ray diffractometer (XRD, Philips, Cu Kα, Ni Kβ) with a speed of scanning of 1° 2θ/min from 20 to 50° and IR spectrum (Buck 500, KBr) with the range of 500–4000 cm^{-1}. TGA/DTA measurement was performed in air using the TGA2950 (TA instruments, USA). Sample weighing 8.01 ± 0.1 mg were heated in a platinum sample cell up to 950 °C at 10°C/min. Ca, K, P, O, and C elemental analyses were measured using Energy-Dispersive X-ray Analysis (EDXA) (Philips PW 2400 X-Ray Fluorescence Spectrometer) and by quantitative analysis (QA). EDXA: W/W %: K 18.8%, Ca 27.5%, P 6.8%, C 5.8%. QA: W/W %: K 18.3%, Ca 26.9%, P 7.0%, C 5.5%.

Measurement of particle size

Scherrer and Williamson–Hall formulas [38, 39] were used for determination of particle size and micro-strain of KHA powder. Moreover, distribution of particle size was distinguished by TEM (Leo 912 AB, Germany) method. Sample preparation of TEM: first, ultrasonic dispersion of the KHA powder was done in absolute ethanol and then deposited on a copper grid.

Adsorption process and kinetics data

The CR dye (Merck) was dissolved into deionized water that each test was performed by the fresh dilutions. Studying the adsorption mechanism and determining the optimum conditions of CR adsorption were performed using 100 ml of CR with the prepared certain concentrations of KHA samples shaken at 300 rpm at R.T. The adsorbent dosage effect about 0.02–0.5 mg (natural *p*H, 180 min as contact time, room temperature) was examined. The 0–180 min as contact time was applied (60 mg dosage of CR, natural pH, and room temperature). The *p*H effect about 6–12 units was studied. The 20–150 mg L^{-1} as primitive concentrations of CR considered for drawing the charts of adsorption process. The adsorbed concentrations of CR were specified using a UV–Vis spectrum (UNICO 2800) as $\lambda_{max} = 485$ nm. The capacity of equilibrium absorbance [q_e (mg/g)] and quantity of adsorbed CR per unit of adsorbent mass at *t* time were measured using the below formulas:

$$q_e = \left(C_0 - C_e\right)V/m \quad (1)$$

$$q_t = \left(C_0 - C_t\right)V/m \quad (2)$$

$$\text{Removal efficiency } (\%) = 100 \times \left(C_0 - C_e\right)/C_0, \quad (3)$$

where C_0, Ce, and C_t (mg/L) are primitive, equilibrium, and CR concentrations at t time, respectively. V (L) is the dye solution volume, and m (g) is the absorbent mass. The nano-particles of KHA remove total CR of the respected solution, which the color of adsorbed solution obviously reduced. The kinetic data of CR adsorption were evaluated by performance of the respected experiments.

Micro-organisms

The antibacterial activity of the prepared material was examined against three Gram-positive bacteria, namely, *Staphylococcus aureus* ATCC 25923, *Enterococcus faecalis* ATCC 14506, *Staphylococcus coagulase*, and four bacteria of Gram-negative type contains *Escherichia coli* ATCC 25922, *Klebsiella pneumonia* ATCC13883, *Proteus vulgaris* ATCC 33420, *Pseudomonas aeruginosa* ATCC27853. All the microorganisms were provided from Microbiology laboratory culture collection of Sabzevar Medical Science University.

Minimum Inhibitory Concentration Assay (MIC)

The MIC assay was carried out according to the previous studies [40]. Briefly, first, the 96 numbers of well plates (8 × 12 wells) were administered using 100 µl of the culture media (MHB), 100 µl of dispersing mixture of KHA in water used to charging the first well, in following 100 µl of every of the serial dilutions was delivered into sequential wells, and eventually every well loaded with 50 µl of the MHB and 50 µl of the bacteria inoculums which was described earlier. The terminal volume in every well was 200 µl with concentrations of 1000, 500, 250, 125, 62.5, 31.2, 15.6, and 7.8 µg/mL for the compounds and the positive controls (chloramphenicol and ampicillin). Each plate was only used for one microorganism. Three well in the last line of the plate were used as growth controls by filling 50 µl of inoculums and 150 µl of MHB. In addition, three wells used as a negative control by filling 200 µl of MHB. The incubation process about covered plates was performed at 37.5 °C during 24 h. The turbidity of each well was then observed and recorded. The MIC was assessed as the least concentration that inhibited visible growth. All tryouts were done in triplicate [40, 41].

Results and discussion

As an extension of our continued interest in the preparation of new nano-materials bearing some potential applications, herein, a new KHA was for the first time synthesized by the sol–gel method showing as the efficient adsorbent for CR as well as antibacterial behavior [42–44].

Characterization of KHA

XRD analysis

Based on Fig. 1a, the XRD pattern of KHA sample displays the intensive peaks of apatite (AP) structure and shows good identity with the ICDD standards (JCPDS). The AP indices [(002), (211), (301), (302), and (222)] and CaO indices [(200), (230), and (111)] confirm the hexagonal and cubic Bravais systems for them, respectively. Entirely, prepared KHA shows desired crystallinity. The governing of the process of heat-treating and aging steps of sol–gel method helps to polymerization reaction progress between Ca, K, and P precursors that lead to decreasing of the possible impurities' phases [42–44]. Actually, herein, hydrolysis of TEP used in this study as an advantage in comparison with the other ones [45, 46] makes the polymerization reactions more completed and reducing the impurity phases (Eq. 4):

$$\begin{aligned} &OP(OEt)_{3-x}(OH)_x + Ca^{2+} + K^+ + NO_3^- \\ &\quad \rightarrow \left(NO_3\right)^-(OH) - -Ca - -O - -K \\ &\quad - -PO(OEt)_{3-x} + H^+ + C_2H_5OH + H_2O. \end{aligned} \quad (4)$$

Based on literature reports and related diffraction patterns, it can be disclosed which potassium can be doped in the AP structure without permanent changes in the behavior of AP phase in spite of small discrepancies of lattice parameters [47, 48]. The results of X-ray diffraction analysis of the calcined KHA powder show the diffraction patterns resemblance to HAp, although the molar ratio of Ca/P was less than the pure HAp stoichiometric one as 1.67 [37]. The substituted K^+ monovalent ion for Ca^{2+} in the AP structure makes the misbalancing charge that can be neutralized by substitutions of anions like substitution of PO_4^{3-} by CO_3^{2-} or creating supplementary vacancies [49].

FTIR spectra

FTIR spectra can prospect the surface functional groups of KHA particles (Fig. 1b). In addition, the spectra of KHA sample calcined at 300 °C displays the bands at 475, 575, 966, 1090–1220, and 3370 cm^{-1} attributted to stretching modes of phosphate and O–H functional groups, respectively (see Fig. 1b). The appearance band of 1660 cm^{-1} (see Fig. 1b) related to stretching mode of C=O of CO_3^{2-} group indicates the incorporation of carbonate in AP structure improving the absorption character of KHA. The recorded IR spectrum shows resemblance with the similar articles [50].

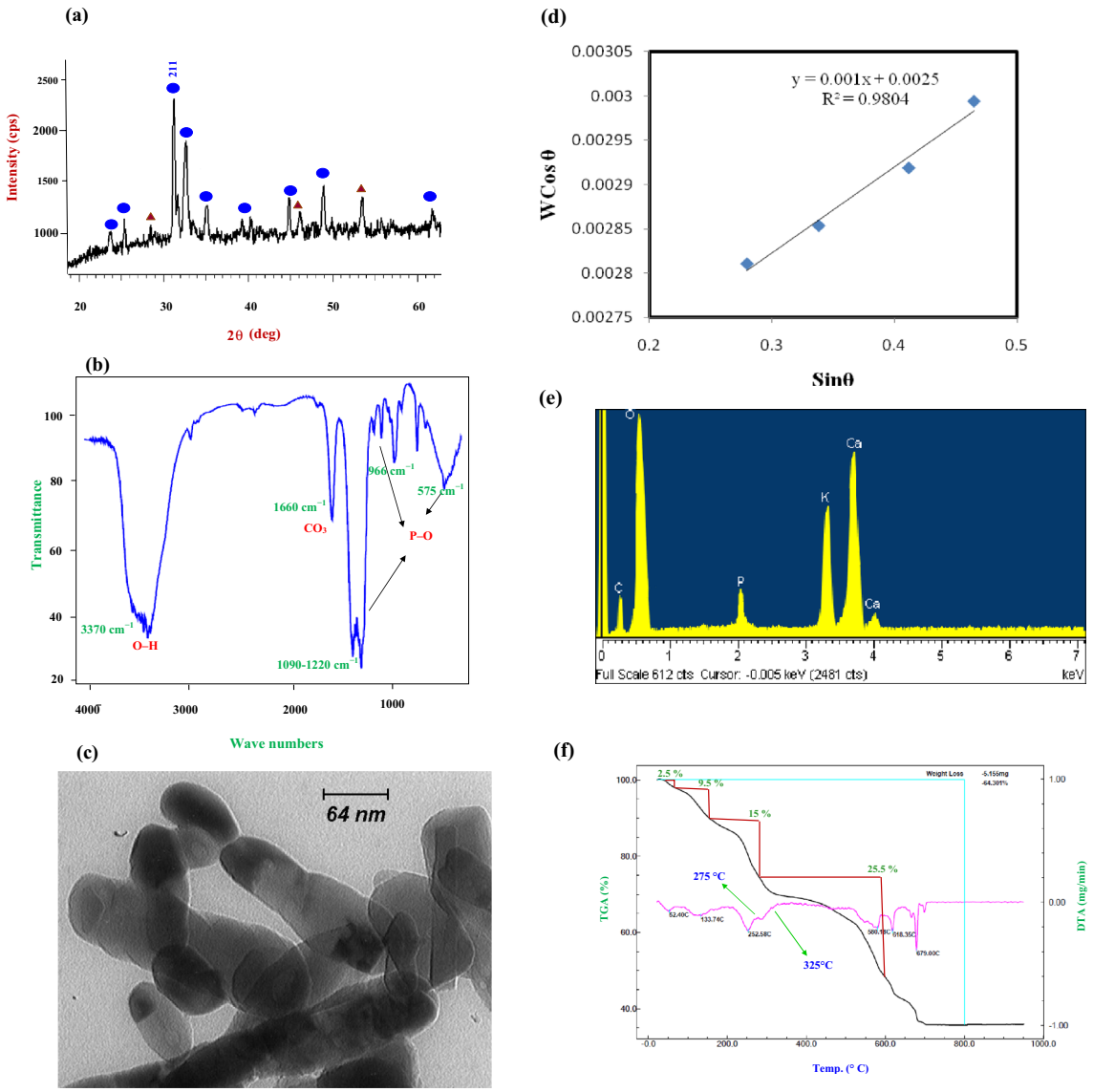

Fig. 1 **a** X-ray diffraction patterns of KHA calcined at 300 °C, shown: (blue circle) HA (red triangle) $CaCO_3$, **b** FTIR of KHA calcined at 300 °C, **c** TEM image of KHA sample, and **d** W–H plot drawn using Cauchy approximation, **e** EDXA and **f** TGA/DTA measurements

Nanostructural examination

Sol–gel technique makes gells with small particles bearing intense surface energy that with the low calcination temperatures the highly agglomerated crystals having the remarkable porosity are prepared. Median particle size of KHA determined by TEM (direct method) and XRD (indirect method) in amount of 65–70 nm (see Fig. 1c) with good consistency. The Scherrer formula (Eq. 5) used for measuring the particle size [42–44, 51]:

$$D = K\lambda / [W\mathrm{Cos}(\theta)], \quad (5)$$

where K equals to 0.9 a constant value, λ is the Cu Kα radiation (0.1544 nm), W is the full-width at half-maximum, and θ is the angle of diffraction (deg).

It is known that the size of crystalline, micro-strain ϵ_s, and the instrument effect influences on peak width of the pattern [50]. Knowing Williamson–Hall (W–H) formula as precise one to deconvolution of size and instrumental effect has been used with the aid of Cauchy approximation (Eq. 6) (for more information, see the literature [39, 42, 43]):

$$(W\mathrm{Cos}\theta) = (K\lambda/D) + 4\epsilon_s \mathrm{Sin}\theta. \quad (6)$$

Crystallite size (D) and ϵ_s can extracted from plot the respected W–H curve of (WCos θ) vs Sin θ for (002), (211), (302), (303), and (222) indices. The measured results are $D = 72$ nm and $\epsilon_s = 2.5\text{E}{-4}$ (cf. Fig. 1d). The elemental specification of EDXA suggested the (Ca + K)/(P + C) molar ratio of 1.69 with $(Ca_{2.94}K_{2.06})(PO4)_{0.94}(CO3)_{2.06}(OH)_1$

formula that established the carbonated KHA preparation (see Fig. 1e).

Thermal analysis of KHA

The TGA/DTA analysis of synthesized KHA is depicted in Fig. 1f. The weight losses in four observed stages. The first one related to 2.5% weight loss recorded in the range of 30–60 °C because of OH group presence. The second and third regions attributed to a 9.5 and 15% weight loss that were observed at the range of 60–150 and 150–275 °C that is because of entrapped chemisorbed water; therefore, amorphous apatite phase changed to crystalline hexagonal phase. The last stage corresponded to 25.5% weight loss observed in the range of 275–600 °C, due to decomposition of impurities like carbonates. DTA shows endothermic peaks in the temperature regions of 252.6, 580.2, 618.3, and 679.0 °C that the first one related to adsorbed surface water and the last three ones correspond to the below suggested reaction:

$$1/2Ca_2P_2O_7 + Ca_3(PO_4)_2 + Ca(NO_3)_2 + CaCO_3 + 1/2H_2O\ Ca_5(PO_4)_3(OH) + CaO + 2NO_2 + CO_2 + 1/2O_2. \quad (7)$$

Moreover, there are two exothermic peaks at 275 and 325 °C are attributed to crystallization process of amorphous to crystallize apatite phases.

Influenced factors about adsorption of CR on KHA

Adsorbent dosage affected on the removal efficiency

The effect of 0.02–0.5 g dose range of KHA on the CR elimination was evaluated for 100 ml solution of CR at 298 K and natural *p*H. As drawn in Fig. 2a, enhancement of adsorbent dosage rapidly increases the dye percentage removal because of the increase of the amount of adsorption sites of KHA. 0.2 g of dosage made the highest CR equilibrium adsorption (98.43%). However, after the equilibrium, the increase of the adsorbent dosage does not increase the removal efficiency of CR. It can be concluded that the saturation of the superlative sites of adsorption, using higher amount of adsorbent causes to some of sites to be wasted. In accordance with obtained results (see Fig. 2a), 0.1 g can be introduced as the optimal adsorbent dosage of CR for the next examinations.

Influence of primitive pH on the removal efficiency

The effect of primitive pH of a series of sample solution on the removal efficiency was tested at 100 mg L^{-1} initial

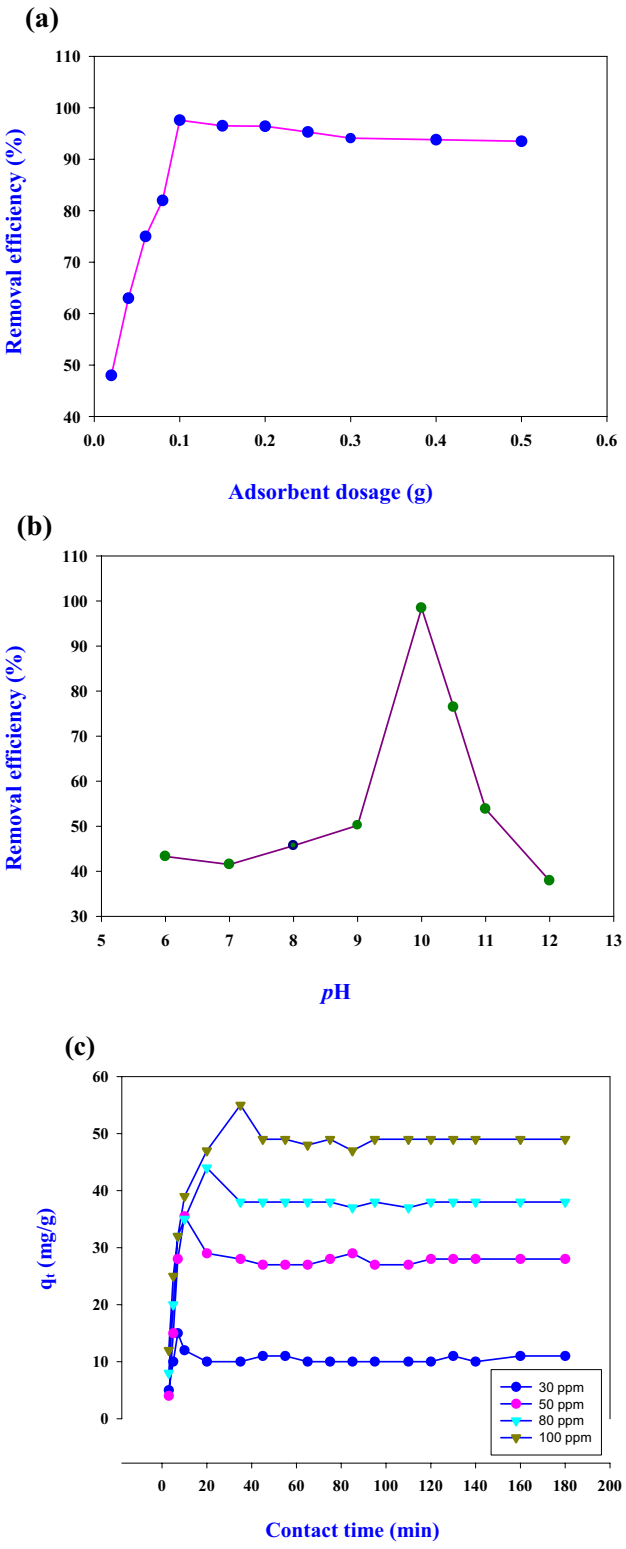

Fig. 2 **a** Effect of dosage, **b** pH, **c** initial dye concentrations on removal efficiency and CR dye adsorption onto sol–gel-derived KHA ($V = 100$ mL, $t = 140$ min, initial *p*H 10, adsorbent dose 2 g/L, and temperature 298 K)

concentration of 100 ml solution of CR in the *p*H range of 6–12 (see Fig. 2b). The pH values less than 6 turn CR molecule to acidic form having the blue color solution (*p*Ka = 3–5). Moreover, the structure of KHA is not stable in solution with pH < 6. The higher quantity removal of CR (98.72%) was established at pH = 10. Therefore, pH = 10 proposed as the optimal pH for the next experiments. The determined point of zero charge (pH_{pzc}) value of KHA sample was 11.5. The CR anionic character and the amphoteric character of AP surface depend on *p*H and control the dye adsorption process. Therefore, stored positive charge over surface of absorbent maybe provides convenient conditions for better CR elimination. As a result, with a gradual increase of solution *p*H, the groups of hydroxyl and phosphate of KHA surface deprotonated and make the electrostatic interactions between opposite charges powerless. However, lesser solution *p*H contents than pH_{pzc} makes positive charge of absorbent surface [52] that provides more intense attraction of the positive absorbent and the negative CR along with the promotion of CR adsorption (see Fig. 2b). Analogous results about adsorption of CR onto further adsorbents have been observed [53, 54].

Influence of contact time and concentration of primitive dye

Figure 2c depicts the results of contact time effect and different primitive dye concentrations (i.e., 20, 30, 50, and 100 ppm, 100 mL) on the absorption of CR dye by 2 g/L KHA nano-particles at pH = 10. Enhancing the primitive concentration of CR is, growing of the capacity of adsorption is, increasing the amount of dye removal efficiency is, and vice versa that augments the primitive adsorbed concentration of CR from 15 to 55 mg/g. Quick growing of adsorption happens during the first 5–30 min and in following slowly goes forward to achieve equilibrium about 37 min for all of the examined samples and for various concentrations of dye. The first rapid adsorption is due to the availability of the adsorbent positive sites, resulting to attraction of the negative charged of CR dye. It can be concluded that 37 min is enough to achieved equilibrium which this time will apply about the next adsorption experiments.

Kinetics data

Kinetic study of dye adsorption rate investigates about the influence of contact time onto adsorption capacity of the adsorbent. Herein, the adsorption process of 100 ppm concentration of CR within the synthesized KHA in *p*H 10 was performed to optimize the wastewater treatment (the results depicted in Fig. 3a). As expected and mentioned, superior enhancing the contact time augments the removal efficiency because of preparing the higher useful time for CR dye absorption. Achieving the equilibrium took 37 min (see Fig. 2c). The mechanism and kinetics of CR adsorption over the new synthesized sol–gel-derived KHA tested about the some known kinetic models as below: The obtained kinetic parameters are depicted in Fig. 3b–f and Table 1.

(1) Pseudo–first-order formula:

$$\log\left(q_e - q_t\right) = \log q_e - k_1 t. \tag{8}$$

(2) Pseudo-second-order formula:

$$t/q_t = \left(1/k_2 q_e^{\,2}\right) + t/q_e. \tag{9}$$

(3) Elovich formula:

$$q_t = (1/\beta)\ln(\alpha\beta) + (1/\beta)\ln t. \tag{10}$$

(4) Bangham formula:

$$\ln q_t = \ln k_b + (1/M)\ln t. \tag{11}$$

(5) Intra-particle diffusion formula:

$$q_t = k_{dif} t^{0.5} + C, \tag{12}$$

where q_e and q_t (mg g^{-1}) are the value of adsorbed CR onto the adsorbent surface at equilibrium and t times (min), respectively. k_1 and k_2 (mg min g^{-1}) are the rate constants of Eqs. (9) and (10). α (mmol g^{-1} min^{-1}) as the rate of primitive adsorption and β (g $mmol^{-1}$) as the constant of desorption are defined. M and k_b are the Bangham model constant. k_{dif} (mg g^{-1} $min^{-0.5}$) is the rate constant of intra-particle diffusion. The calculated values of the mentioned rate constants, respective linear fitted plots, and their correlation coefficients are demonstrated in Fig. 3 and are listed in Table 1.

The obtained results confirm the desirability of pseudo-first-order kinetic equation within rate of adsorption of CR dye ($R^2 = 0.9867$). According to the linear fitting plotted of CR adsorption, process of intra-particle may be an alternative rate determining step of CR elimination by KHA (see Fig. 3f). Therefore, this diffusion model should offer useful information about the diffusion mechanism. However, the plot depicted in Fig. 2c shows that reaction of dye adsorption advanced according to these below steps (1) 37 min as first part of dye adsorption on exterior adsorbent layer; (2) during 55 min, next gradual adsorption proceeds via intra-particle diffusion; and (3) and the last step is equilibrium adsorption. Alike results for CR adsorption onto another adsorbents are reported by others [53–56].

Adsorption charts

The adsorption procedure continues to achieve the dynamic equilibrium of the adsorbed molecules of adsorbate and the residual one in the solution. The adsorption charts make clear the correlation of these two values and explaining the

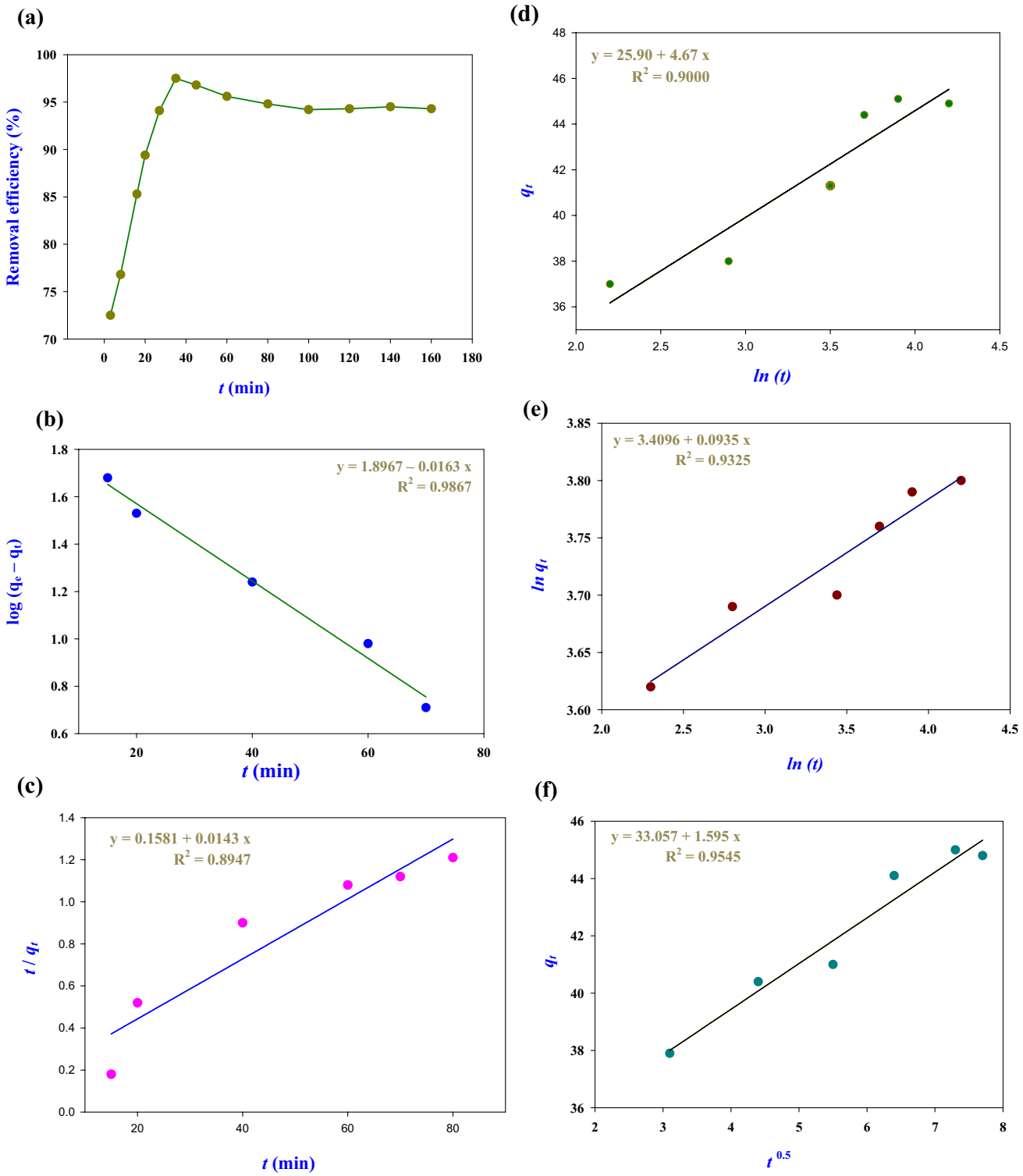

Fig. 3 **a** Effect of contact time on the removal efficiency, **b** pseudo-first-order kinetics, **c** pseudo-second-order kinetics, **d** Elovich kinetics, **e** Bangham kinetics, and **f** intra-particle diffusion kinetics for CR onto CaHA ($C^0 = 100$ mg L^{-1}, $V = 100$ mL, $t = 0$–140 min, temperature at 298 K)

interactions between adsorbate and surface of adsorbent gives important physicochemical data within the procedure of adsorption. There are numerous for adsorption that explains the experimental data. In this study, the isotherm models of Henry, Langmuir, Freundlich, and Temkin were applied at 298, 308, and 318 K as below:

Table 1 Constants and correlation coefficients for adsorption kinetic models of CR dye

Kinetic model	Parameters	100 ppm CR	R^2
Pseudo-first order	k_1 (mg min g^{-1})	0.0163	0.9867
	q_e (mg g^{-1})	87.832	
Pseudo-second order	k_2 (mg min g^{-1})	0.0013	0.8947
	q_e (mg g^{-1})	63.930	
Elovich	α (mmol $g^{-1}min^{-1}$)	1197.3	0.9000
	β (g $mmol^{-1}$)	0.214	
Bangham	M	10.70	0.9325
	k_b (mg g^{-1})	30.25	
Interparticle diffusion	k_{dif} (mg g^{-1} $min^{1/2}$)	1.595	0.9545

(1) Henry equation:

$$q_e = K_H C_e. \tag{13}$$

(2) Langmuir equation:

$$1/q_e = \left(1 / \left(b\, q_m C_e\right)\right) + 1/q_m. \tag{14}$$

(3) Freundlich equation:

$$\ln q_e = \ln K_F + (1/n) \ln C_e. \tag{15}$$

(4) Temkin equation:

$$q_e = \left(RT/b_T\right)\left(\ln C_e + \ln A_T\right), \tag{16}$$

where q_m and qe (mg/g) are the superlative monolayer and equilibrium capacities, respectively. Intensity and capacity of adsorption could be described by K_H and K_F constants. C_e (mg/L) is the aqueous CR equilibrium concentration, b is the coefficient of Langmuir equilibrium (L/mg), the empirical parameter of constant n shows the adsorption process favorability, and heat and interaction energy of adsorption procedure analyzed by equilibrium constants of A_T and b_T, respectively. These used isotherm models illustrated in Fig. 4 and the exported slope and intercept data are listed in Table 2. The simplest linear adsorption isotherm resembles Hendry's law that the amount of the surface of adsorbate is represented to be proportional to the C_e of adsorbent. The Langmuir and Freundlich isotherms suppose that the adsorbate occupies the adsorbent homogeneous and heterogeneous sites, respectively [57]. Temkin isotherm describes the adsorbent–adsorbate interactions based on the heat of adsorption procedure (function of temperature) that linearly decrease [58].

Regarding the correlation coefficient, Langmuir model well explains the experimental data of CR equilibrium adsorption ($R^2 = 0.9939$ at 298 K; $R^2 = 0.9962$ at 308 K; $R^2 = 0.9936$ at 318 K). Based on these obtained results, increase of temperature causes the decreasing of superlative CR adsorption capacity of KHA. The most adsorption capacity of synthesized KHA was measured 505.19 mg/g at 298 K. Hall et al. [59] using a dimensionless constant R_L (Hall separation factor) show the desirability of an adsorption procedure based on the Langmuir model:

$$R_L = 1 / \left(1 + bC_0\right), \tag{17}$$

where C_0 is the most primitive dye concentration in the solution (mg/L). The values of R_L confirm that charts are irreversible ($R_L = 0$), undesirable ($R_L > 1$), favorable ($0 < R_L < 1$), or linear ($R_L = 1$). In this work, the obtained data (for $C_0 = 100$ mg/L) in the range of $0 < R_L < 1$ are 0.1927, 0.2421, and 0.2370 at 298, 308, and 318 K, respectively (see Table 2). Therefore, the adsorption of CR over KHA is desirable. However, $0 < 1/n < 0.5$ expresses that CR adsorbs easygoing on the synthesized KHA. In addition, the correlation coefficient (R^2) of Temkin equation was more than two alternatives ones (Henry and Freundlich) as higher than 0.8882 at the applied three temperatures meaning adsorption process remarkable influenced by heat.

Assessment of performance

The highest capacities of CR dye adsorption over the new synthesized KHA material and for other known adsorbents using Langmuir isotherm are depicted in Table 3. In accordance with the gained data of $q_{m,}$ it may be concluded that this new introduced KHA is an adsorbent with high capability within the aqueous CR obliteration, being as powerful industrial absorbent compared with the current ones (see Table 3 and refs. inside). In addition, adsorption of CR by KHA is a quick process achieved instantly to equilibrium condition for 30 ppm and about 2 min for 50 ppm and 4 min for 80 ppm, and indicates that KHA has high potential for purification of environmental wastewater. The interesting issue of this new absorbent is its impressive capacity of adsorption at ambient temperature, although improvement of many of the other reported compounds needs to *p*H or temperatures changing.

Antibacterial study

According to the results of MIC assay, which are shown in Table 4, KHA exhibited excellent antibacterial activity. The compound prevented the growth of all bacteria strains. However, its activity was less than the positive control of chloramphenicol. KHA inhibited the growth of *S. aureus, S. coagulase, E. coli*, and *K. pneumonia* with the lowest concentration of 125 µg/mL. The ability of the compound in this assay may be due to the presences of functional groups of phosphate, hydroxyl, and carbonate groups and also the particle size of the KHA, which have been previously reported as the functional group and factors for antibacterial activity of nano-materials [65–70]. Many research groups have investigated the antimicrobial mechanisms of metallic compounds. The physical and

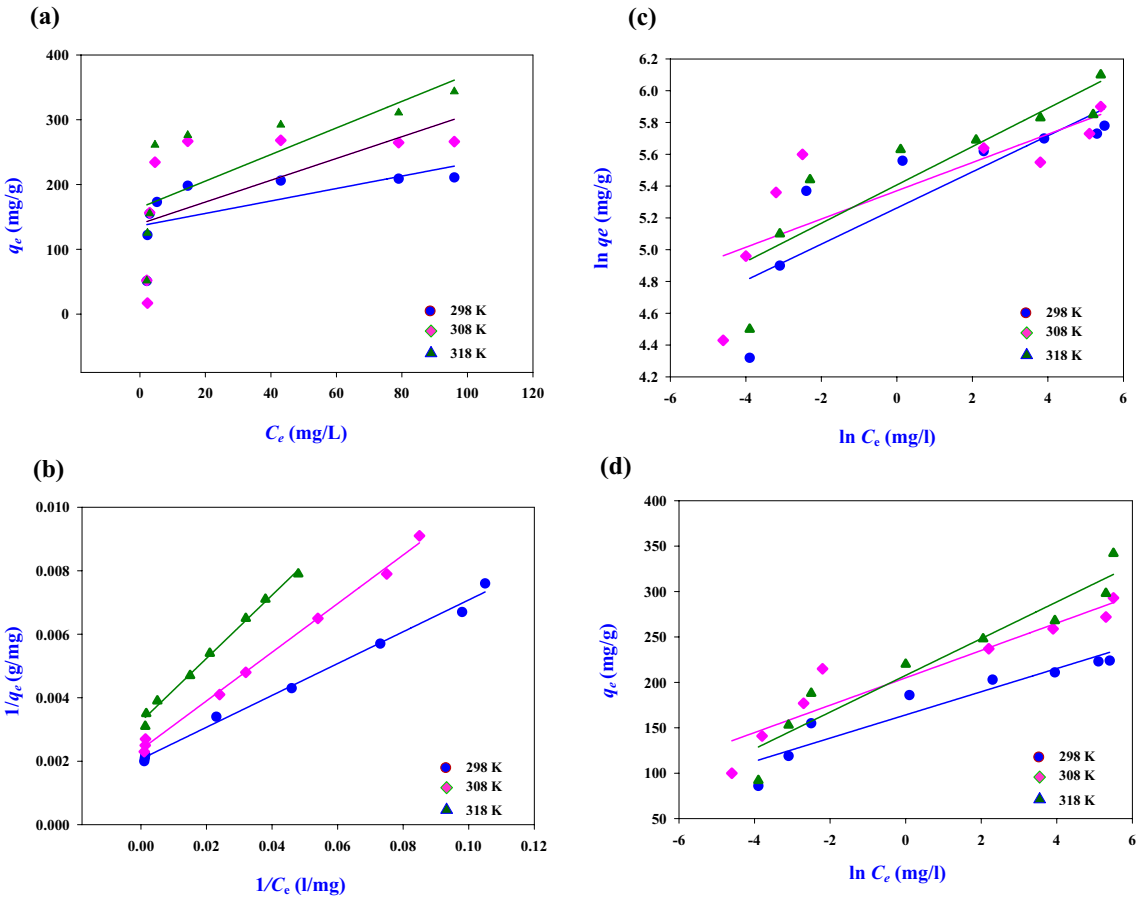

Fig. 4 **a** Henry, **b** Langmuir, **c** Freundlich, and **d** Temkin adsorption isotherms fit of CR onto CaHA (C_0 = 20–100 mg L^{-1}, V = 100 mL, contact time for 30 min, *p*H at 10, temperature at 298 K, 308 K, and 318 K)

Table 2 Adsorption isotherm constants and correlation coefficients for adsorption of CR on sol–gel-derived KHA at 298 K, 308 K, and 318 K (initial pH 6, adsorbent dose 2 g/L, and contact time 30 min)

Adsorption Isotherm	Parameters	Temperature (K)		
		298	308	318
Henry	K_H	0.1437	0.1851	0.2347
	R^2	*0.5680*	0.5832	*0.6420*
Langmuir	b	0.0419	0.0313	0.0322
	q_m	505.19	437.67	348.50
	R^2	*0.9939*	*0.9962*	*0.9936*
Friendlich	K_F	192.94	215.01	223.07
	$1/n$	0.1137	0.0889	0.1206
	R^2	*0.7202*	*0.6252*	*0.7930*
Temkin	b_T	194.11	169.98	130.76
	A_T	3847	8108	2883
	R^2	*0.8910*	*0.8882*	*0.9184*

Table 3 Comparison of maximum adsorption capacity (q_m) of CR by various adsorbents determined using Langmuir adsorption isotherm model

Adsorbent	q_m (mg/g)	CR concentration (mg/L)	Reference
Calcined KHA	505.19	20–100	This work
Ag (0.5): CaHAp	458.08	50–300	[30]
Ca bentonite	107.41	50–200	[60]
$Ni_{0.6}Fe_{2.4}O_4$	72.73	5–60	[61]
CS-M-GMCNTS	262.9	10–60	[62]
$CoFe_{1.93}Gd_{0.07}O_4$	263.16	25–120	[63]
Hollow Zn–Fe_2O_4 nanospheres	16.1	1–50	[17]
Starch–AlOOH–FeS_2	333.33	50–500	[64]

chemical properties of both the metal atoms and the accessible donor ligands influenced biomolecules. Metal species have predictable behavior and participate in spatially localized or discrete reactions that abolish enzyme activities, disrupt membrane function, or damage DNA [71, 72]. Sun et al. have

Table 4 Minimum inhibition concentration (MIC) for KHA values given in µg/mL

Strain name	KHA	Positive control[a]
Gram positive		
Staphylococcus aureus	125.0 ± 0.0 [b]	25.0 ± 0.0
Staphylococcus coagulase	125.0 ± 0.0	25.0 ± 0.0
Enterococcus faecalis	250.0 ± 0.0	25.0 ± 0.0
Gram negative		
Escherichia coli	125.0 ± 0.0	25.0 ± 0.0
Klebsiella pneumonia	125.0 ± 0.0	25.0 ± 0.0
Proteus vulgaris	250.0 ± 0.0	25.0 ± 0.0
Pseudomonas aeruginosa	250.0 ± 0.0	25.0 ± 0.0

[a]Chloramphenicol

[b]Values are presented as means ± SD ($n = 3$)

proposed that slow release metal ion sterilization and photocatalytic sterilization are the principal reasons for antibacterial mechanism of KHA material [73].

Conclusions

In the present work, an ordinary sol–gel method was used to synthesize the nano-particles of new potassium-substituted HA, and then, its structure characterized and particle size measured using XRD, FTIR, EDXA, TGA/DTA, and TEM analyses. The revised Scherrer's formula and TEM technique determined the average particle size as 65–70 nm. The KHA well accomplished for adsorption of CR as a very rapid procedure that reached to steady state less than 2 min. The KHA adsorbent within CR works better at lesser temperatures. The KHA optimal CR adsorption at 298 K was measured in amount of 505.19 mg/g, well matched by Langmuir equation with $R^2 > 0.9939$. In the base of kinetic results, the data well matched with pseudo-first-order formula. The most important results obtaining in this paper, one can find that herein, sol–gel-obtained KHA may be used as inexpensive and biocompatible effectual adsorbent for CR elimination from environment. MIC assay results demonstrate the excellent antibacterial activity of KHA. It shows the growth inhibition of *S. aureus, S. coagulase, E. coli*, and *K. pneumonia* bacteria around the lowest concentration of 125 µg/mL.

Acknowledgements MCH gratefully acknowledges the financial support by the Hakim Sabzevari University. M.M. gratefully acknowledges the financial support by the Ferdowsi University of Mashhad.

References

1. L.L. Lian, L.P. Guo, C.J. Guo, Adsorption of Congo red from aqueous solutions onto Ca-bentonite. J. Hazard. Mater. **161**, 126–131 (2009)
2. M.S. Sajab, C.H. Chia, S. Zakaria, S.M. Jani, M.K. Ayob, K.L. Chee, P.S. Khiew, W.S. Chiu, Biores. Technol. **102**, 7237 (2011)
3. B. Saha, S. Das, J. Saikia, G. Das, J. Phys. Chem. C **115**, 8024–8033 (2011)
4. N. Zaitseva, V. Zaitsev, A. Walcarius, Chromium (VI) removal via reductionesorption on bi-functional silica adsorbents. J. Hazard. Mater. **250**, 454–461 (2013)
5. R. Ahmad, R. Kumar, Appl. Surf. Sci. **257**, 1628 (2010)
6. C.T. Benatti, C.R.G. Tavares, E. Lenzi, Sulfate removal from waste chemicals by precipitation, J. Environ. Manage. **90**, 504–511 (2009)
7. K.P. Gopinath, S. Murugesan, J. Abraham, K. Muthukumar, Bioresour. Technol **100**, 6295 (2009)
8. A.A. Pel_aez-Cida, I. Vel_azquez-Ugaldeb, A.M. Herrera-Gonz_alezc, J. García- Serranoc, Textile dyes removal from aqueous solution using Opuntia ficus-indica fruit waste as adsorbent and its characterization. J. Environ. Manag. **130**, 90–97 (2013)
9. S. Saber-Samandari, S. Saber-Samandari, M. Gazi, Cellulose-graft-polyacrylamide/ hydroxyapatite composite hydrogel with possible application in removal of Cu (II) ions. React. Funct. Polym. **73**, 1523–1530 (2013)
10. F. Zhang, B. Ma, X. Jiang, Y. Ji, Powder Technol. **302**, 207–214 (2016)
11. M. Mohandes, M.H. Salavati-Niasari, Z. Fathi, Fereshteh, Mater. Sci. Eng.: C **45**, 29–36 (2014)
12. F. Mohandes, M. Salavati-Niasari, Chem. Eng. J. **252**, 173–184 (2014)
13. F. Mohandes, M. Salavati Niasari, Mater. Sci. Eng.: C **40**, 288–298 (2014)
14. K. Diouri, A. Kherbeche, A. Chaqroune, Int. J. Innovative Res. Sci., Eng. Technol. **4**, 267–274 (2015)
15. W. Wen, J.M. Wu, Eruption, ACS Appl. Mater. Interfaces. **3**, 4112–4119 (2011)
16. C. Xia, Y. Jing, Y. Jia, D. Yue, J. Ma, X. Yin, Desalination **265**, 81 (2011)
17. L. Wang, J. Li, Y. Wang, L. Zhao, Q. Jiang, Chem. Eng. J. **181**, 72–79 (2012)
18. M. Bhaumik, R. McCrindle, A. Maity, Chem. Eng. J. **228**, 506 (2013)
19. H. Hou, R. Zhou, P. Wu, L. Wu, Chem. Eng. J. **336**, 211–212 (2012)
20. M.I. Kay, R.A. Young, Nature **204**, 1050 (1964)
21. A. Amiri, M. Chahkandi, A. Targhoo, Analytica Chimica Acta **950**, 64–70 (2017)
22. K.G. Scheckel, G.L. Diamond, M.F. Burgess, J.M. Klotzbach, M. Maddaloni, B.W. Miller, C.R. Partridge, S.M. Serda, J. Toxicol. Environ. Health B Crit. Rev. **16**, 337 (2013)
23. K.L. Lin, J.Y. Pan, Y.W. Chen, R.M. Cheng, X.C. Xu, J. Hazard. Mater. **161**, 231 (2009)
24. M. Chahkandi, A.A. Amiri, S.R. Saadatdar Arami. Microchem. J. **144**, 261–269 (2019)
25. M. Zargazi, M.H. Entezari, Appl. Catal. B: Environ. 242 (2019) 507–517
26. M. Zargazi, M.H. Entezari, Ultrason. Sonochem. **51**, 1–11 (2019)
27. M. Zargazi, M.H. Entezari, J. Photochem. Photobiol. A: Chem. 365 (2018) 185–198
28. S. Zinatloo-Ajabshir, S. Mortazavi-Derazkola, M. Salavati-Niasari, Ultrasonics Sonochem. 42 (2018) 171–182
29. S. Zinatloo-Ajabshir, S. Mortazavi-Derazkola, M. Salavati-Niasari, J. of Mole. Liq. **231**, 306–313 (2017)
30. M. Safari-Amiri, S. Mortazavi-Derazkola, M. Salavati-Niasari, S.M. Ghoreishi **28**, 6467–6474 (2017)
31. Y. Tang, H.F. Chappell, M.T. Dove, R.J. Reeder, Y.J. Lee, Zinc incorporation into hydroxylapatite. J. Biomater. **30**, 2864–2872 (2009)

32. G. Liu, J. Talley, C. Na, S. Larson, L. Wolfe, Copper doping improves hydroxyapatite sorption for arsenate in simulated groundwaters. Environ. Sci. Technol. **44**, 1366–1372 (2010)
33. C. Srilakshmi, R. Saraf, Microporous Mesoporous Mater. **219**, 134–144 (2016)
34. C. Wei, H. Zhiliang, L. Yu, H. Qianjum, Preparation and characterization of a novel solid base catalyst hydroxyapatite loaded with strontium. Catal. Commun. **9**, 516–521 (2008)
35. E.S. Bogya, R. Barabas, A. Savdari, V. Dejeu, I. Baldea, Hydroxyapatite modified with silica used for sorption of copper (II). Chem. Pap. **63**, 568–573 (2009)
36. C.H. Suelter, Enzymes activated by monovalent cations. Science **168**, 789–795 (1970)
37. H.J. Hohling, H. Mishima, Y. Kozawa, T. Daimon, R.H. Barckhaus, K.D. Richter, Microprobe analyses of the potassiumcalcium distribution relationship in predentin, Scanning Microsc. Int. **5**, 247–253 (1991)
38. S. Kannan, J.M.G. Ventura, J.M.F. Ferreira, Ceram. Int. **33**, 1489–1494 (2007)
39. G.K. Williamson, W.H. Hall, Acta Metall. **1**, 22–31 (1953)
40. A. Knauth, Chem. Mater. **17**, 2378–2385 (2005), F. Boulc ̀h
41. W. Mahdavi, L.B. Yaacob, I. Din, Nazlina, Antimicrobial activity of consecutive extracts of Etlingera brevilabrum. Sains Malaysiana **41**, 1233–1237 (2012)
42. M. Baghayeri, B. Mahdavi, Z. Hosseinpor-Mohsen, S.Farhadi Abadi, Green synthesis of silver nano-particles using water extract of Salvia leriifolia: antibacterial studies and applications as catalysts in the electrochemical detection of nitrite. Appl. Organomet. Chem. **32**, 4057 (2018)
43. H. Eshtiagh-Hosseini, M.R. Housaindokht, M. Chahkandi, Mater. Chem. Phys. **106**, 310–316 (2007)
44. M. Chahkandi, Mater. Chem. Phys. **202**, 340–351 (2017)
45. K. Cheng, W. Weng, G. Han, P. Du, G. Shen, J. Yang, J.M.F. Ferreira, Mater. Chem. Phys. **78**, 767–771 (2003)
46. W. Cheng, G. Weng, P. Han, G. Du, J. Shen, J.M.F. Yang, Ferreira, Mater. Res. Bull. **38**, 89–97 (2003)
47. H.El Feki, T. Naddari, J.M. Savariault, A. Ben Salah, Localization of potassium in substituted lead hydroxyapatite: Pb9.30K0.60(PO4)6(OH)1.20 by X-ray diffraction. Solid State Sci. **2**, 725–733 (2000)
48. E.G. Nordstrom, K.H. Karlsson, Chemical characterization of a potassium hydroxyapatite prepared by soaking in potassium chloride and carbonate solutions. Biomed. Mater. Eng. **2**, 185–189 (1992)
49. H.El Feki, A. Ben Salah, A. Daoud, A. Lamure, C. Lacabanne, Studies by thermally stimulated current (TSC) of hydroxyl and fluoro-carbonated apatites containing sodium ions. J. Phys. Condens. Matter **12**, 8331–8343 (2000)
50. L. Cui, Y. Wang, L. Hu, L. Gao, B. Du, Q. Wei, RSC Adv. **5**, 9759–9770 (2015)
51. H. Borchert, E.V. Shevchenko, A. Robert, I. Mekis, A. Kornowski, G. Grübel, H. Weller, Langmuir. **21**, 1931–1936 (2005)
52. A. Harding, N. Rashid, K.A. Hing, Biomaterials, 26 (2005) 6818
53. L. Guangci, S. Yuanyuan, L. Xuebing, L. Yunqi, RSC Adv. **6**, 11855–11862 (2016)
54. G. Bharath, A. Jagadeesh Kumar, K. Karthick, D. Mangalaraj, C. Viswanathan, N. Ponpandian, RSC Adv. **4**, 37446–37457 (2014)
55. C. Ng, J.N. Losso, W.E. Marshall, R.M. Rao, Bioresour. Technol. **85**, 131–135 (2002)
56. B. Serap Cetınkaya, Akkaya, Mater. Sci. Eng.: C **68**, 573–578 (2016)
57. H.M.F. Freundlich, Z. Phys. Chem. **57**, 385 (1906)
58. M.I. Tempkin, V. Pyzhev, Acta Phys. Chim. USSR **12**, 327–356 (1940)
59. K.R. Hall, L.C. Eagleton, A. Acrivos, T. Vermeulen, Ind. Eng. Chem. Fundam. **5**, 212 (1966)
60. L. Lian, L. Guo, C. Guo, J. Hazard. Mater. **161**, 126–131 (2009)
61. S. Zeng, S. Duan, R. Tang, L. Li, C. Liu, D. Sun, Chem. Eng. J. **258**, 218–228 (2014)
62. H.Y. Zhu, Y.Q. Fu, R. Jiang, J. Yao, L. Liu, Y.W. Chen, L. Xiao, G.M. Zeng, Appl. Surf. Sci. 285 B (2013) 865–873
63. X.R. Zhao, W. Wang, Y.J. Zhang, S.Z. Wu, F. Li, J.P. Liu, Chem. Eng. J. **250**, 164 174 (2014)
64. R. Kumar, J. Rashida, M.A. Barakat, RSC Adv. **4**, 38334–38340 (2014)
65. E. Kolanthai, K. Ganesan, M. Epple, S.N. Kalkura, Synthesis of nanosized hydroxyapatite/agarose powders for bone filler and drug delivery application. Mater. Today Commun. **8**, 31–40 (2016)
66. S. Mortazavi-Derazkola, M. Salavati-Niasari, H. Khojasteh, O. Amiri, S.M. Ghoreishi, Green synthesis of magnetic Fe_3O_4/SiO_2/HAp nanocomposite for atenolol delivery and in vivo toxicity study. J. Clean. Prod. **168**, 39–50 (2017)
67. F. Mohandes, M. Salavati-Niasari, Journal of nanoparticle research 16 (2014) 2604&#8207
68. F. Mohandes, M. Salavati-Niasari, RSC Adv. **4**, 25993–26001 (2014)
69. J.T. Ratnayake, M. Mucalo, G.J. Dias, Substituted hydroxyapatites for bone regeneration: a review of current trends. J. Biomed. Mater. Res. Part B: Appl. Biomater. **105**, 1285–1299 (2017)
70. B. Tian, W. Chen, Y. Dong, J.V. Marymont, Y. Lei, Q. Ke, Y. Guo, Z. Zhu, Silver nanoparticle-loaded hydroxyapatite coating: structure, antibacterial properties, and capacity for osteogenic induction in vitro. RSC Adv. **6**, 8549–8562 (2016)
71. J.A. Lemire, J.J. Harrison, R.J. Turner, Antimicrobial activity of metals: mechanism, molecular targets and applications. Nat. Rev. Microbiol. **11**(6), 371 (2013)
72. A. Rajendran, R.C. Barik, D. Natarajan, M. Kiran, D.K. Pattanayak, Synthesis, phase stability of hyd roxyapatite–silver composite with antimicrobial activity and cytocompatability. Ceram. Int. **40**(7), 10831–10838 (2014)
73. D. Sun, M. Babar Shahzad, M. Li, G. Wang, D. Xu, Antimicrobial materials with medical applications. Mater. Technol. **30**, B90–B95 (2015)